Drivers of air-sea CO_2 flux in the subantarctic zone revealed by time series observations

Xiang Yang[1,2], Cathryn A. Wynn-Edwards [2,4], Peter G. Strutton[1,3], Elizabeth H. Shadwick[2,4]

[1]Institute for Marine and Antarctic Studies, University of Tasmania, Hobart, TAS, Australia
[2]Australian Antarctic Program Partnership, Hobart, TAS, Australia
[3]Australian Centre for Excellence in Antarctic Science, University of Tasmania, Hobart, TAS, Australia
[4] CSIRO, Hobart, TAS, Australia

Corresponding author: Xiang Yang (xiang.yang@utas.edu.au), ORCiD: 0000-0002-0616-0967

Key points:

- A MLR model was built based on SOTS data, to simulate surface pCO_2 in the Australian sector SAZ over the last 20 years.
- Biological productivity controls the seasonal variability of pCO_2, and drives a net carbon sink over two decades.
- Mesoscale processes, and to a lesser extent, the Southern Annular Mode, drive local air-sea CO_2 flux variability.

Abstract

The subantarctic zone is an important regions in the Southern Ocean with respect to its influence on air-sea CO_2 exchange and the global ocean carbon cycle. However, understanding of the magnitude and drivers of the flux are still being refined. Using observations from the Southern Ocean Time Series station (~47°S, 142°E) and auxiliary data, we developed a multiple linear regression model to compute the sea surface partial pressure of CO_2 (pCO_2) over the past two decades. The mean amplitude of the pCO_2 seasonal cycle between 2004 and 2021 was 44 µatm (range 30 to 54 µatm). Summer minima ranged from 310 to 370 µatm and winter maxima near equilibrium with the atmosphere. The non-thermal (i.e. biological processes and mixing) contribution to the seasonal variability in pCO_2 was several times larger than the thermal contribution. The SOTS region acted as a net carbon sink at annual time scales, with a mean magnitude of 6.0 mmol m^{-2} d^{-1}. The positive phase of the Southern Annular Mode (SAM) increased ocean carbon uptake primarily through an increase in wind speed at zero time lag. Increased surface pCO_2 was correlated with a positive SAM with a lag of 4 months, mainly due to reduced biological uptake and increased mixing. During the autotrophic season, pCO_2 was predominantly impacted by primary productivity, while water mass movement, inferred by temperature and salinity anomalies, had a larger impact in the heterotrophic season. In general, mesoscale processes such as eddies and frontal movement impact the local biogeochemical features more than the SAM.

1. Introduction

The Southern Ocean has a significant influence on Earth's climate by absorbing a large amount of anthropogenic heat and taking up both natural and anthropogenic carbon dioxide (CO_2; Devries, 2014; Lenton et al., 2013; Sabine et al., 2004; Takahashi et al., 2009). Oceanic carbon uptake from the atmosphere depends in part on biological consumption and solubility of CO_2 in seawater. These processes are influenced by seasonal surface forcing or water mass movement or both (Takahashi et al., 2002, 2009). Although the Southern Ocean carbon sink is important, there is still large uncertainty about its magnitude (Gruber et al., 2019). Landschützer et al. (2015) and Le Quéré et al. (2007) suggested that the Southern Ocean carbon sink weakened from the 1980s to the early 2000s. Despite its apparent recovery after that, it seems to have weakened again since 2011 (Keppler & Landschützer, 2019). While the spatial coverage of in-situ measurements has increased dramatically (Bushinsky et al., 2019; Gray et al., 2018; Takahashi et al., 2009), disagreements among the global carbon models (Hauck et al., 2020; Lenton et al., 2013) remain, and the magnitude of the Southern Ocean carbon sink is still being refined (Bushinsky et al., 2019; Gray et al., 2018).

The Southern Ocean Time Series (SOTS) site is located southwest of Tasmania and considered representative of the Subantarctic Zone (SAZ) between 90°E and 140°E (Figure 1; Trull et al., 2001) based on remote sensing and the regional oceanography. The SOTS observatory provides long-term, high-frequency hydrographic sensor records (temperature, salinity), discrete measurements (dissolved inorganic carbon, phytoplankton composition), and also continuous partial pressure of carbon dioxide (pCO_2) records in the sea and atmosphere (Shadwick et al., 2021; Wynn-Edwards et al., 2020).

Based on previous studies we divided the Southern Ocean into zones by different ocean fronts and for this work we will focus on the SAZ, the region between the Subtropical and Subantarctic Fronts (Figure 1). The subduction of Subantarctic Mode Water (SAMW) in the SAZ makes an important contribution to the uptake of anthropogenic CO_2 (Sabine et al., 2004). The well-mixed, oxygen-rich SAMW spreads equatorward to supply oxygen and nutrients that support global ocean productivity (Sarmiento et al., 2004; Shadwick et al., 2015). Although the SAZ has relatively low surface dissolved iron concentrations (Bowie et al., 2009; Lannuzel et al., 2011), the biologically-mediated surface CO_2 depletion is the primary driver of the annual net CO_2 uptake by the region (Lenton et al., 2013; Shadwick et al., 2015).

The Southern Annular Mode (SAM) is the dominant mode of extratropical southern hemisphere climate variability (Fogt & Marshall, 2019; Lovenduski & Gruber, 2005). It is characterized by large-scale changes in atmospheric mass between the mid and high latitudes, related to the location and strength of westerly winds (Lenton & Matear, 2007; Lovenduski & Gruber, 2005). A poleward shift of westerly winds to higher latitudes is thought to increase upwelling in the Antarctic Zone (AZ), increasing northward Ekman transport from the AZ and southward Ekman transport from the Subtropical Zone (STZ). Together, these lead to convergence in the SAZ, increasing both downwelling and mixed layer depth (MLD; Lovenduski et al., 2007; Lovenduski & Gruber, 2005). The correlation between SAM and parameters like chlorophyll concentration, wind speed, sea surface temperature (SST), carbon flux is generally weak in the SAZ because of the regional differences (Keppler & Landschützer, 2019; Lovenduski et al., 2007; Lovenduski & Gruber, 2005; Sallée et al., 2010). Moreover, the SOTS site is at the junction of two regions with contrasting response to the positive SAM, and thus poorly represented by global scale models (Figure 1 in Lovenduski & Gruber, 2005; Sallée et al., 2010).

Here we present a multiple linear regression model based on high-frequency sea surface pCO_2 measurements from the SOTS site, augmented by Argo and remote sensing data, to estimate pCO_2 from 140 to 144°E; 48 to 46°S around the SOTS mooring (Figure 1) over the past two decades. The resulting time series is used to characterize the seasonal cycle, interannual variability and the decadal trend of the surface pCO_2 and also to quantify the air-sea exchange of CO_2. To assess the impact of the dominant climate mode in this region on the seasonal and interannual variability, correlations between the time series of pCO_2 and the SAM are evaluated. The impact of mesoscale processes on pCO_2 seasonality and air-sea CO_2 exchange is also investigated. This research thus contributes to our understanding of Southern Ocean carbon uptake and can help to refine predictions of future changes in the SAZ.

2. Methods

2.1 Southern Ocean Time Series observations

The Southern Ocean Time Series (SOTS) is a facility of the Australian Integrated Marine Observing System (IMOS; https://imos.org.au/facilities/deepwatermoorings/sots). It is located at approximately 47°S, 142°E, southwest of Tasmania, in the Indian Ocean sector of the SAZ (Figure 1). The SOTS observatory consists of two deep-water moorings, the Southern Ocean Flux Station (SOFS) and the SAZ sediment trap mooring. The SOFS mooring was first deployed in November 2011, with annual turn around and provides high temporal resolution air-sea CO_2 observations in subantarctic waters. Water temperature, salinity, wind speed and chlorophyll fluorescence are measured by instruments on the surface buoy. Surface water and atmospheric pCO_2 are measured by a Moored Autonomous pCO_2 (MAPCO2) system (Sutton et al., 2014), in the surface buoy. Subsurface temperature and pressure data from SOFS is used to define the mixed layer depth (Shadwick et al., 2021; Wynn-Edwards et al., 2020). All SOFS data used here are available from the IMOS AODN portal (https://portal.aodn.org.au/).

2.2 Auxiliary data and regression model inputs

Since the SOTS time series is incomplete and only started in 2011 (Figure 3), auxiliary data from satellites, ships and Argo floats were used to fill the gaps and develop a regression model to extend the pCO_2 time series. Surface chlorophyll concentrations were obtained from the Ocean-Colour Climate Change Initiative (OC-CCI), with resolutions of 8 days and 4 km. This product combines multiple ocean color satellite missions to provide the best quality contemporary data and the longest historical record. SST data were obtained from the NASA Moderate Resolution Imaging Spectroradiometer (MODIS) mission, with the same resolution as chlorophyll. The daily sea level anomalies (SLA) were retrieved from the Copernicus Marine Service with a spatial resolution of 0.25° to identify eddies. These data were averaged to the same 8-day periods as SST.

The Roemmich-Gilson Argo Climatology product was used for full-depth temperature and salinity data, with a spatial resolution of 1° (Roemmich & Gilson, 2009). The ERA5 reanalysis product provided hourly wind speed at 10m height with 0.25° spatial resolution. The Ocean Reanalysis System 5 (ORAS5) provided monthly sea surface salinity (SSS), with 0.25° spatial resolution. Atmospheric mole fractions of CO_2 were taken from the Cape Grim Baseline Air Pollution Station (http://www.csiro.au/greenhouse-gases/) to calculate the air-sea CO_2 fluxes. Monthly SST and mean sea level pressure data from the ERA5 and SSS from ORAS5 were used to convert mole fractions to pCO_2 (Zeebe & Wolf-Gladrow, 2001). The SAM monthly indices were used as per Marshall (2003; https://legacy.bas.ac.uk/met/gjma/sam.html).

To generate an independent time series of pCO_2 with which to evaluate our MLR, upper 10m alkalinity and pH from the Global Ocean Data Analysis Project v2.2022 (GLODAP) were used to calculate pCO_2, using the CO2SYS program (https://github.com/jamesorr/CO2SYS-MATLAB) developed by Lewis & Wallace (1998) and improved by Van Heuven et al. (2011) with the same constants used in (Sutton et al., 2014). We also used data from the Southern Ocean Carbon and Climate Observations and

Modeling Project (SOCCOM; data through end of 2021) profiling float array, taking only observations in the upper 10m used to generate pCO_2. Finally, we removed the SOTS record in the Surface Ocean CO_2 Atlas (v2022, SOCAT) product, to make it independent for validation of the MLR model. All three products (GLODAP, SOCAT and SOCCOM) were subsampled in the region around the SOTS site described below (Figure S1) and averaged monthly for consistency (see section 2.5).

We performed a correlation study between climate indices, observations and MLR model outputs, which required the removal of long term trends and seasonal cycles from the time series. We used the MATLAB function ‘detrend’ to remove the long-term trend, consistent with the recommendation of Sutton et al (2022). And we used the method from Takahashi et al. (2002) to remove the seasonality, which is described in detail in Sutton et al. (2014). This was done for all parameters used in this study. For surface chlorophyll, months with more than 75% missing values, due to gaps in satellite coverage, were taken as empty and linearly interpolated based on the annual cycle before detrending and removing the seasonal cycle.

2.3 Definition of front location and mixed layer depths

The mixed layer depth (MLD) was defined as a 0.2°C temperature change from 10m for both Argo and SOTS estimates (Shadwick et al., 2015; Yang et al., 2022). To help reduce errors due to non-uniform vertical sampling, the Argo data were linearly interpolated to 1m vertical resolution. A polygon (140 to 144°E; 48 to 46°S; Figure 1) was defined around the SOTS site. The monthly averaged chlorophyll, SST, wind speed and MLD were averaged inside the polygon and used as inputs to the MLR model, to construct a hindcast of pCO_2 (eq. 1). The definitions of the STF and SAF were taken from Orsi et al. (1995) and Sokolov & Rintoul (2002) as the potential temperature of 11°C at 150m depth and 4°C at 400m depth, respectively. The potential temperature was calculated from the Argo gridded temperature and salinity using the Gibbs-SeaWater Oceanographic Toolbox (McDougall & Barker, 2011; https://www.teos-10.org/software.htm#1). The time series of frontal positions were averaged in the longitudinal range of 140 to 144°E, to represent the SOTS region.

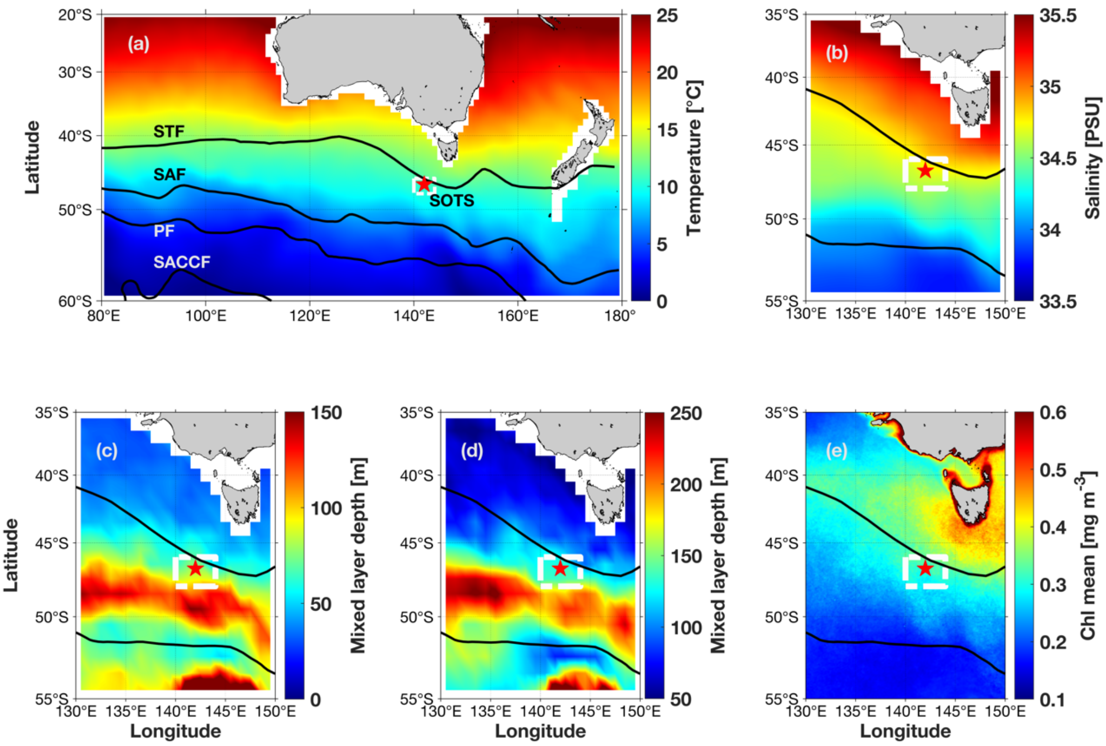

Figure 1. Climatological surface (a) temperature, (b) salinity, and (e) chlorophyll concentration for the period 2004 to 2021. The climatology of MLD (c) during the autotrophic season (October to February) and (d) heterotrophic season (March to September). Climatology was calculated from the auxiliary data described in section 2.2. The general location of the SOTS station is indicated by the red star, and the white polygon represents the area within which the auxiliary data were averaged. Major fronts are indicated in panel (a) following Orsi et al. (1995). They are the Subtropical Front (STF), the Subantarctic Front (SAF), the Polar Front (PF), and the Southern Antarctic Circumpolar Current Front (SACCF).

2.4 Validation of predictor variables and development of the MLR model

Before using the SOTS pCO_2 time series to develop the MLR model, the predictor variables were tested and calibrated based on in-situ data. The relationships between satellite SST, Argo MLD, reanalysis wind speed and their mooring equivalents are approximately 1:1, which confirms that the auxiliary data represent the features in the polygon well (Figure 1 and 2). We acknowledge that the SST measured by SOTS is generally higher than the satellite measurements, but satellite SST captures the seasonality and interannual variability (Figure 2b and S3b), so we use it to build the MLR model. Equally, there appears to be a bias in the MLD measurements (Figure 2d). The gridded Argo product cannot resolve the very deep mixing observed by the mooring, but the seasonality was well captured by it (Figure S3d). The chlorophyll concentrations from SOTS were based on the mooring chlorophyll fluorescence (FChl) at 30m. But in-situ fluorescence can overestimate chlorophyll concentrations and there are gaps in the timeseries (Figure S2; Johnson et al., 2013; Roesler et al., 2017; Schallenberg et al., 2019). For these reasons, we used satellite chlorophyll data in our model. Shipboard High Performance Liquid Chromatography (HPLC) data were compared with the satellite chlorophyll estimates (Roesler et al., 2017; Vives et al., 2022; Wright et al., 2010). Surface (≤ 10m) HPLC pigment samples were collected by the Southern Ocean Large Area Carbon Export (SOLACE) voyage and annual SOTS voyages near the mooring station, which include surface underway and CTD cast data. Although the sample size is modest (N = 14), the relationship (slope = 1.00, $r^2 = 0.52$; Figure 2a and S2) suggests that the satellite measurements capture the surface chlorophyll signal well. At decadal time scales, the seasonality in auxiliary data (except Chl; Figure S3) are consistent with in-situ observations with high-precision reported previously by Shadwick et al. (2015) in their figure 4, but with smaller seasonal magnitude.

We use auxiliary data to derive the following equation for predicting surface ocean pCO_2, subsequently referred to as pCO_2-MLR:

$$pCO_2\text{-MLR} = 435.62 - 51.12*Chl - 8.14*SST - 0.83*U + 0.03*MLD + 0.26*t \quad (1)$$

which represents pCO_2 as a function of chlorophyll (Chl), SST, wind speed (U), MLD and time (t). Time is defined as the number of months since January 2004, to account for the influence of increasing anthropogenic atmospheric CO_2. The coverage length of our MLR model is determined by the longest historical records that all auxiliary products can provide together. In this study, it is limited by Argo gridded products (started in 2004).

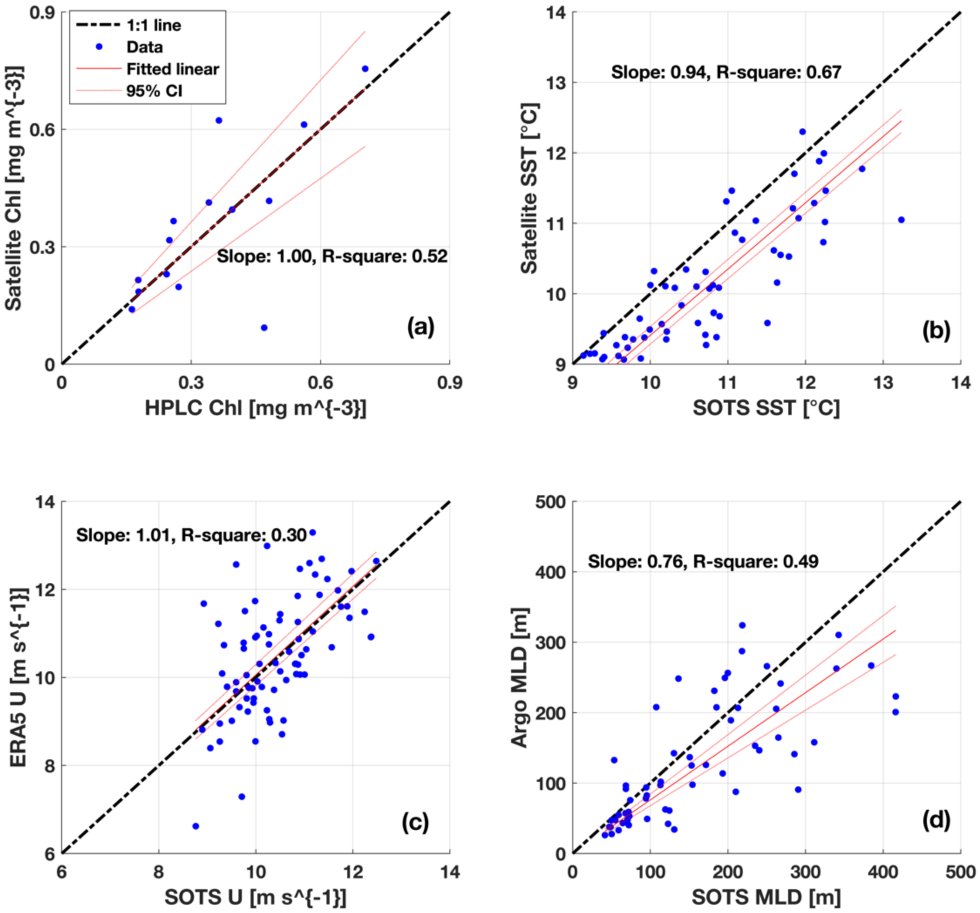

Figure 2. Plots of auxiliary predictor variables versus in-situ measurements. (a) Chlorophyll concentration: OCCCI vs ship-based HPLC, (b) SST: MODIS-Aqua vs SOTS mooring, (c) U at 10m: ERA5 vs SOTS mooring, (d) MLD: RG-Argo vs SOTS mooring. Dashed lines represent the 1:1 relationship, the slope and r^2 of the linear fit (solid red line with dotted line 95% confidence intervals) are included in each subpanel.

2.5 Validation of the MLR model

The MLR model was validated and tested by shipboard measurements and autonomous profiling float estimates (Gray et al., 2018; Williams et al., 2017) of pCO_2 concentration, obtained from GLODAP, SOCCOM and SOCAT. Generally, the long-term increase of pCO_2 from 2012 to 2021 was well captured by the MLR model (Figure 3a). Monthly averaged GLODAP data is in good agreement with the MLR results. Compared with the data from SOTS and SOCAT, our model simulates the seasonal cycle well, especially the whole annual cycle covered by SOTS data from late 2018 to early 2020. Our MLR also correlates very well with the shipboard and float measurements (SOCAT: $r = 0.94$, $p =$

$2.3*10^{-6}$, n = 13; SOCCOM: r = 0.79, p = 0.01, n = 9), which verifies that the model can be used for temporal and spatial extrapolation of pCO_2 (Figure 3a and S1). The value of n is small because it is monthly averaged and subsampled spatially. Compared with SOTS and SOCAT observations, the MLR model underestimates the winter pCO_2, particularly in 2015 and 2017. It is likely that the MLR model misses some short-lived and weak outgassing periods in winter but the impact of these on the net annual fluxes is small.

2.6 Air-sea CO_2 flux and pCO_2 component calculation

The air-sea CO_2 flux (FCO_2) was computed with

$$FCO_2 = k\alpha\Delta pCO_2 \tag{2}$$

where k and α are the gas transfer velocity (Fay et al., 2021) and solubility coefficient (Weiss, 1974) and ΔpCO_2 is the gradient in pCO_2 between the surface water and the atmosphere (ocean minus atmosphere). Negative flux values indicate CO_2 uptake by the ocean. The monthly wind speed, SST and SSS were used to compute coefficients and FCO_2 with the MATLAB function: 'Air-sea CO_2 flux (Chapa, 2022; https://www.mathworks.com/matlabcentral/fileexchange/50190-air-sea-co2-flux)'. The gas transfer velocity is calculated by the monthly average of the squared hourly wind speed. This is done to avoid underestimate the wind speed and its variability.

To understand the contribution of physical and biological drivers to the variability of pCO_2, we separated the influence of temperature (pCO_2-T) and other components (pCO_2-NT) following the empirical relationship of Takahashi et al. (2002) and Landschützer et al. (2018):

$$pCO_2\text{-T} = \overline{pCO_2} \times \exp(0.0423(SST - \overline{SST})) \tag{3}$$

$$pCO_2\text{-NT} = pCO_2 \times \exp(0.0423(\overline{SST} - SST)) \tag{4}$$

where the overbar represents the annual mean value (McKinley et al., 2006; Takahashi et al., 2002). We note that the non-thermal part includes both biological and physical processes (such as upwelling of DIC-rich waters and air-sea exchange of CO_2), but we treat it as an indication of predominantly biological processes and therefore use the terminology pCO_2-NT. For more discussion of the calculation method of pCO_2-NT, refer to section 4.4.

3. Results

3.1 pCO_2 variability and trend

From 2004 to 2021, the mean magnitude of the seasonal cycle (difference between summer minima and winter maxima) of pCO_2-MLR was approximately 44 µatm. The smallest seasonal change (30 µatm) was in 2011 and the largest (54 µatm) was in 2020 (Figure 3). In contrast, seasonal atmospheric pCO_2 variability in the Southern Ocean was less than 10 µatm, because the atmosphere is a large, well-mixed reservoir. The seasonal pCO_2-MLR minima usually occurred in midsummer (December or January). In 2004 it was 310 µatm and in 2021 it was 368 µatm. Maximum values occurred in winter (2004: 361 µatm and 2021: 403 µatm). Decadal trends are also captured by the model. Between 2004 and 2021 pCO_2-MLR increased by 40 µatm in the winter and approximately 60 µatm in the summer (Figure 3). By fitting a linear regression model across the whole study period, the long-term growth rate of the surface ocean pCO_2 at the SOTS site was found to be 2.8 µatm yr^{-1}.

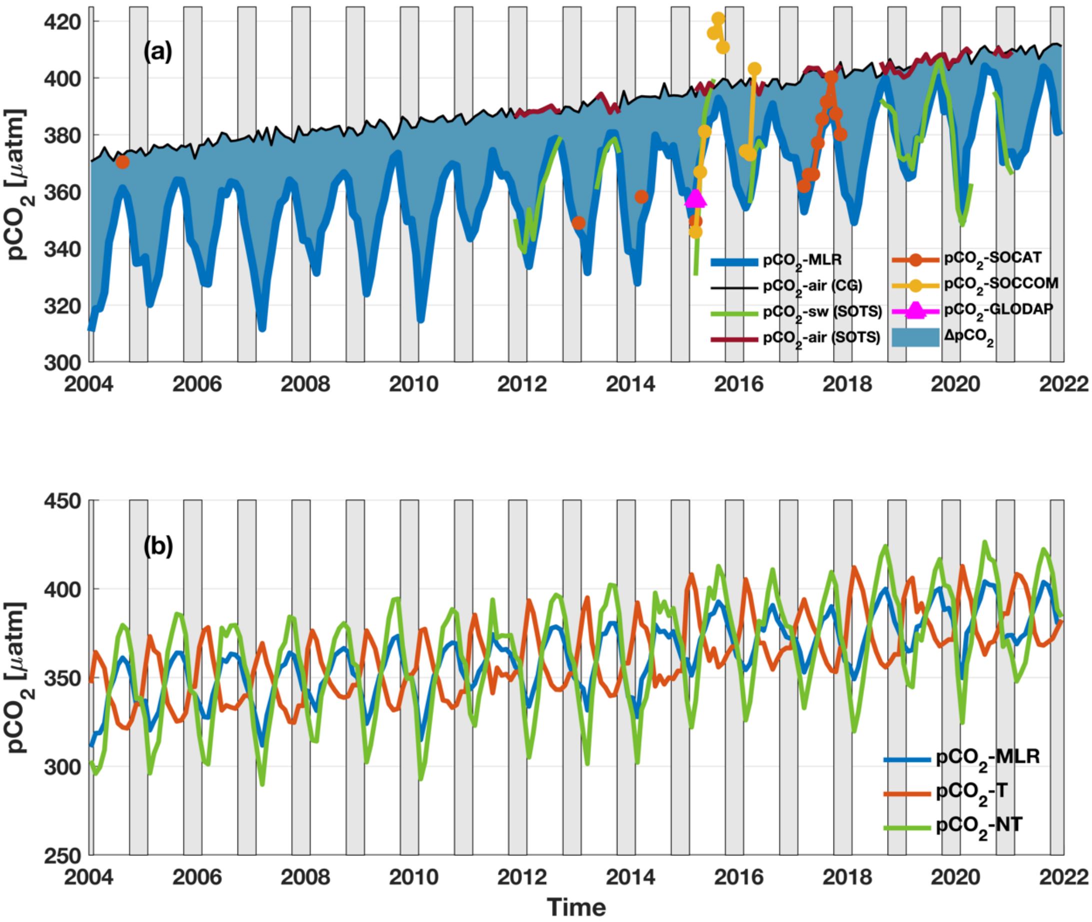

Figure 3. Time series of pCO_2 in the SOTS region. (a) Comparison of observed pCO_2 with pCO_2-MLR. The abbreviations in the figure legend are as follows: pCO_2-MLR is the MLR

model result; pCO_2-air (CG) is atmospheric pCO_2 measured at the Cape Grim (Tasmania) station; pCO_2-sw (SOTS) is sea water pCO_2 measured by the SOTS mooring; pCO_2-air (SOTS) is atmospheric pCO_2 measured by the SOTS mooring; pCO_2-SOCAT/SOCCOM/GLODAP are sea water pCO_2 products; ΔpCO_2 is the gradient between pCO_2-MLR and pCO_2-air (CG), used to calculate FCO_2. (b) Time series of pCO_2-MLR decomposed into thermal and biological components using eq.3 and 4. Gray shading denotes autotrophic season, October to February.

3.2 Physical and biological components

Decomposing the pCO_2-MLR time series into thermal and non-thermal components allows the physical and biological drivers to be explored. Figure 3b shows that the annual cycle is largely influenced by the biological component (pCO_2-NT) which has a magnitude of about 100 µatm (Figure 3b). It is about 2 times larger than the opposing thermal component (pCO_2-T). The pCO_2-NT usually peaks in September, except in years such as 2011 (June), 2015 (August), and sharply decreases during the autotrophic season to a minimum around February (Figure 3b). In the first half of the time series, in 2007 and 2010, there is a very strong reduction of pCO_2-NT, which causes an undersaturation relative to the atmosphere of more than 80 µatm in summer (Figure 3b). By contrast, the magnitude of the summer decrease is especially small in 2008 and 2011, likely due to weak primary production as seen in the negative Chl anomaly in those years (Figure S3).

3.3 Air-sea CO_2 flux, FCO_2

The seasonality of FCO_2 is consistent with that of pCO_2. From 2004 to 2021, this region acted as a net sink for atmospheric CO_2 with an average monthly magnitude of 6.0 mmol m^{-2} d^{-1} (~26.5 g C m^{-2} y^{-1}). The strongest sink period is from February to April, with a maximum value of -16.0 mmol m^{-2} d^{-1} and an average value of -9.1 mmol m^{-2} d^{-1} with standard deviation of 2.1 mmol m^{-2} d^{-1} (Figure 4). During the winter and early spring, FCO_2 is at a minimum, and it decreases from about -6 mmol m^{-2} d^{-1} to about -3 mmol m^{-2} d^{-1} from July to September (mean value: -3.1 mmol m^{-2} d^{-1} and standard deviation: 1.4 mmol m^{-2} d^{-1}; Figure 4). The FCO_2 is most variable in summer, and more stable in winter but the winter magnitude over the last few years has decreased to near zero. In general, the SOTS region is a sink for atmospheric CO_2 (Figure 4).

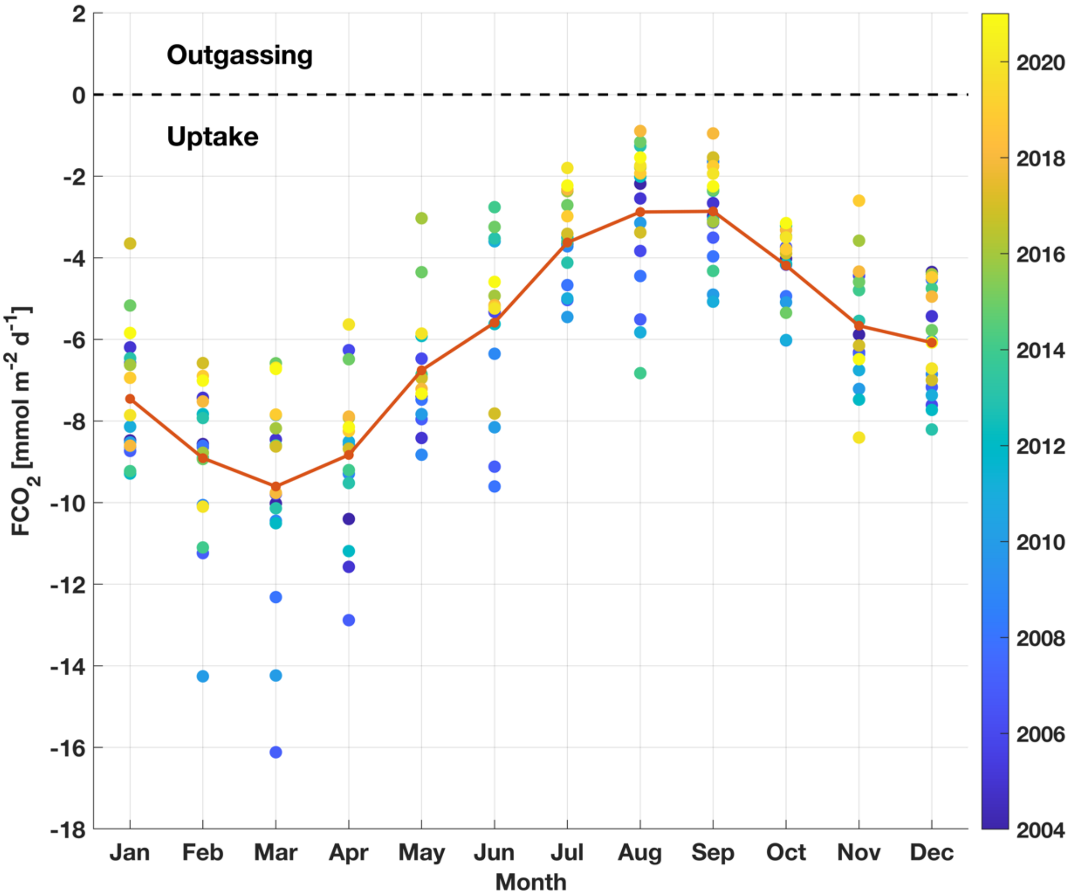

Figure 4. The air-sea CO_2 flux by month of year. Color scale is blue to yellow from past to present, 2004 to 2021. The orange solid line indicates the average value for each month. Negative values indicate ocean uptake of CO_2.

3.4 Correlation with the SAM index

Pearson correlation tests were performed between the SAM index and each parameter, the significant results were shown in Table 1, with a time lag of 0 to 6 months to detect any delayed impact of the SAM. First, the predictor variables Chl and SST did not significantly correlate with the SAM index at any time lag. The SAM was positively correlated with wind speed with no time lag ($r = 0.18$, $p = 0.01$) and a similar result was observed for MLD at 1 month lag ($r = 0.18$, $p = 0.01$), indicative of a positive SAM co-occurring with stronger wind induced mixing (Table 1). The SAM was also positively correlated with surface pCO_2-MLR with a lag of 4 months ($r = 0.15$, $p = 0.02$), and we observed a similar result for the nonthermal component (pCO_2-NT; Table 1). Also, the SAM was positively correlated with the magnitude of the oceanic uptake of CO_2 (shown here by negative FCO_2) with no lag. As seen for MLD, the enhanced ocean CO_2 uptake is related to the SAM-wind result just described (r = -0.16).

Table 1. The correlation test results for parameters with SAM index for 2004 to 2021. Note here we only show the significant results.

	r	p	Time lag
Wind speed	0.18	0.01	0 month
FCO_2	-0.16	0.02	0 month
Mixed layer depth	0.18	0.01	1 month
pCO_2-MLR	0.15	0.02	4 months
pCO_2-NT	0.17	0.01	4 months

3.5 Drivers of pCO_2 variability across seasons

The pCO_2-MLR time series was divided into two seasons to explore what drives pCO_2 variability, especially potential effects of temperature and primary productivity. We define October through February as the autotrophic season (austral spring and summer), when primary production dominates and the surface ocean is warming. March through September as the heterotrophic season (austral autumn and winter), when respiration and upward mixing of carbon rich subsurface waters dominate. During the autotrophic season, pCO_2-NT was mostly influenced by primary production, as seen by the negative correlation with chlorophyll concentration (Figure 5a). During the heterotrophic season, the pCO_2-NT anomaly varied from about -20 μatm to 20 μatm with very small chlorophyll variation, which implies that other processes are important during this season and are included in the pCO_2-NT component (Figure 5b). During this period, the pCO_2-NT anomaly was negatively correlated with SST, as shown by the increasing warm color with the negative SST anomaly (Figure 5c). It was also generally positively related to the MLD, shown by the increasing warm color with the positive MLD anomaly on the x-axis of Figure 5d. This suggests that the upwelling or mixing of DIC-rich subsurface water mainly increased surface pCO_2 in the heterotrophic season. This could potentially increase SSS, but in our case, the pCO_2-NT anomaly was not closely related to SSS anomaly (Figure 5c). As for the

pCO_2-T anomaly, it varies linearly with the SST anomaly over the whole year, the variability of pCO_2-T was most prominent between 2013 and 2015 (Figure S4).

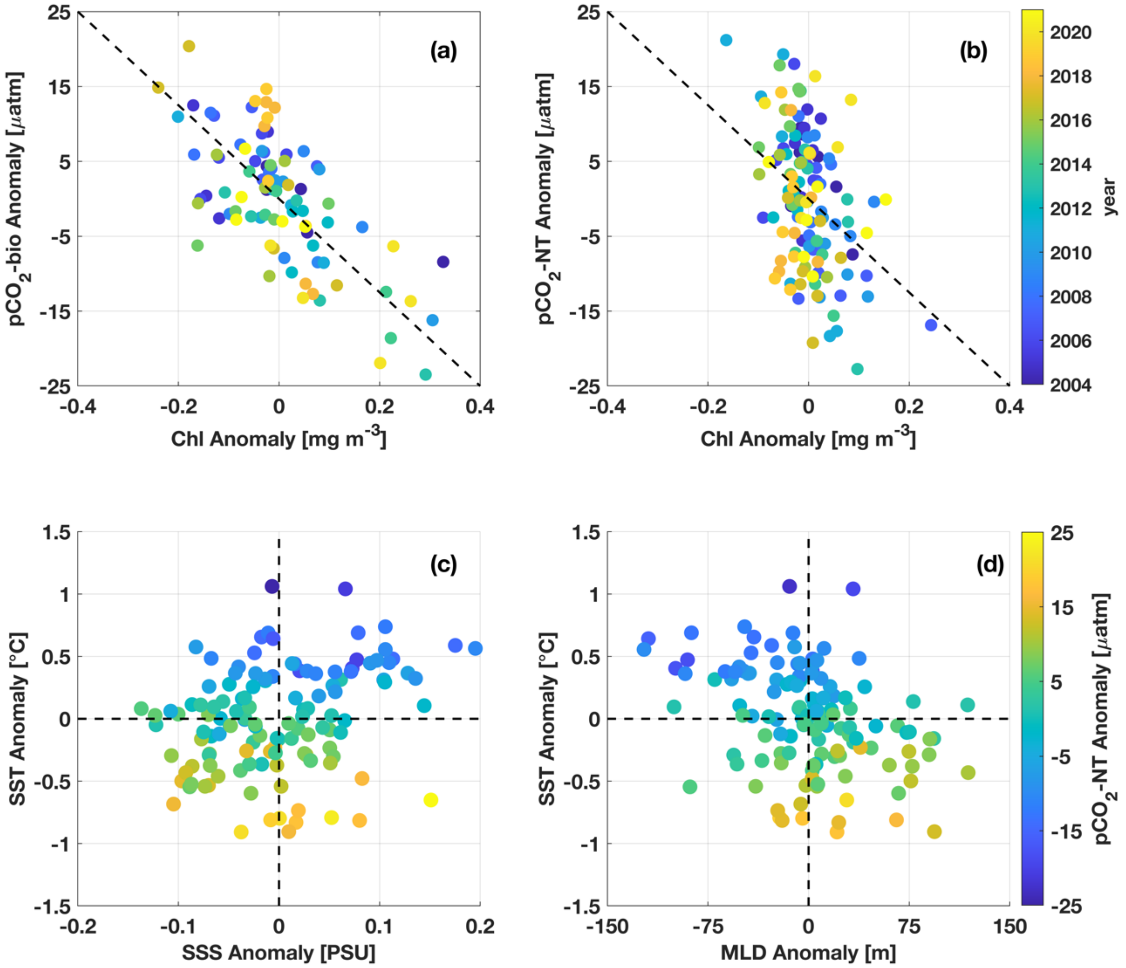

Figure 5. The relationship between anomalies of pCO_2-NT and Chl in (a) autotrophic and (b) heterotrophic seasons. Relationship of pCO_2-NT with combinations of (c) SST and SSS, (d) SST and MLD anomalies, during the heterotrophic seasons.

3.6 Case studies

The weak correlation between SST, chlorophyll and SAM implies other potential drivers for temperature and chlorophyll anomalies besides prominent climate modes. Water masses moving into the study area from south or north, driven by STF movement and mesoscale structures, are likely to influence the local hydrography and pCO_2 (Figure 1; Prend et al., 2022; Shadwick et al., 2015). We used case studies to investigate in detail the connections between the SAM, biological and physical drivers, and variability of pCO_2 (Figure 6). Three two-year periods were selected to include different phases of the SAM to explore its influence: 1) 2009 to 2010, negative SAM index transitions to positive index; 2) 2015 to 2016, positive SAM index; 3) 2019 to 2020, negative SAM index. SLA and SST were used to identify eddies (Figure 7); an animation for the whole case study period is presented in the Supporting Information package. Since pCO_2-NT contributes a large proportion of the variability in pCO_2-MLR (Figure 3 and 5), it is the focus of this section.

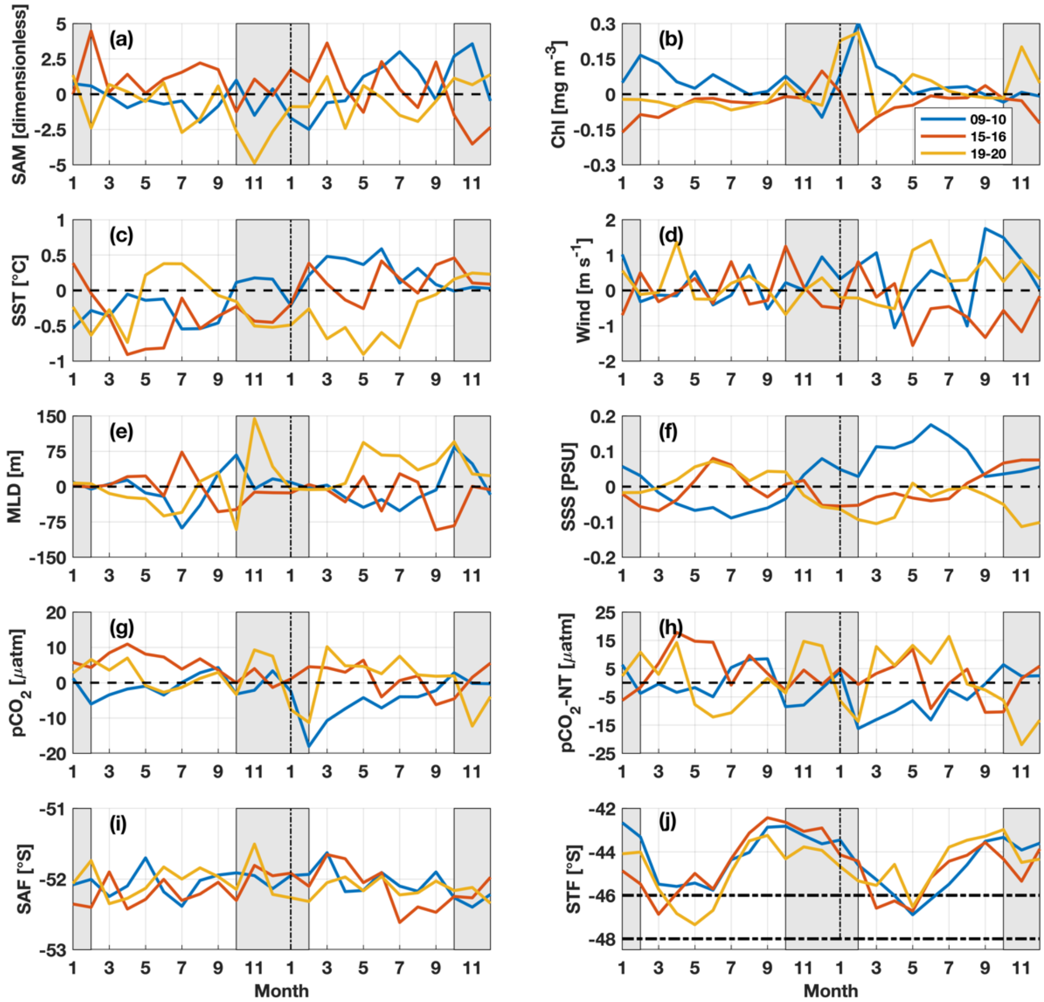

Figure 6. Anomalies for case studies described in section 3.6: (a) SAM index, (b) Chl, (c) SST, (d) U, (e) MLD, (f) SSS, (g) pCO_2-MLR, (h) pCO_2-NT. Frontal position of (i) subantarctic front (SAF) and (j) subtropical front (STF). The black dashed lines in (j) represent the boundaries of the box defined in Figure 1. 09-10: from 2009.1 to 2010.12; 15-16: from 2015.1 to 2016.12; 19-20: from 2019.1 to 2020.12. Gray shading denotes the autotrophic season, October to February.

Through comparing the three typical SAM cases (positive, negative and transition), we found that neither persistent SAM nor changing SAM resulted in obvious changes to the SOTS region (Figure 6). This reinforces the correlation test results in section 3.3. Four drivers mainly influenced the pCO_2-NT variability: (1) biological activity; (2) deep mixing; (3) STF movement; (4) eddy activity, or interactions between these (Figure 6 and 7). Over the whole case study, the biological activity seems to dominate the pCO_2 variation in the autotrophic season. The strongest negative pCO_2-NT anomalies occurred in February 2010, January and February 2020, and November 2020 and they all overlapped with a strong Chl increase (Figure 6b and 6h). One exception to this occurred in November 2019, when a significant pCO_2-NT increase overlapped with strong MLD deepening (Figure 6 and S5). The other negative pCO_2-NT anomalies appeared in June 2019 and June 2010 and are discussed in the next paragraph.

The effect of frontal movement lasts longer but is less intense when compared to biological activity. As seen in Figure 6i and 6j, the STF played a more important role than the SAF to control the water masses entering the SOTS region with strong seasonality. It is especially clear in the case of 2009 to 2010. As the STF moves north, SOTS is farther south within the SAZ. This water mass is cooler and fresher, with higher DIC, which resulted in the slightly increase of pCO_2-NT from July to September (Figure 1 and 6). When the STF returned south and passed the SOTS region in 2010, it was followed by warmer and saltier subtropical water, with low DIC, leading to negative pCO_2-NT anomalies from around March to July (Figure 6). This mechanism might reduce the pCO_2-NT persistently after the strong biological drawdown in February.

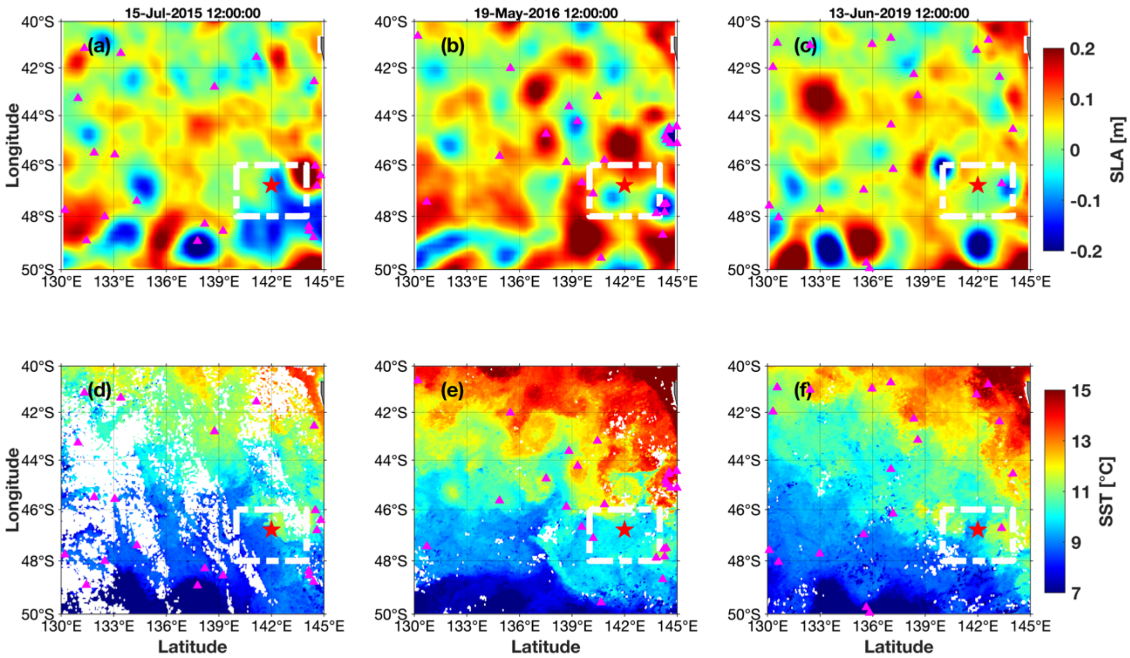

Figure 7. 8-day (a, b and c) SLA and (d, e and f) SST maps of the study region around (a, d) 2015/7/15, (b, e) 2016/5/19 and (c, f) 2019/6/13. The time stamp is the median of the 8 days period. The magenta triangles denote the location of Argo floats during the same time window. The general location of the SOTS station is indicated by the red star, and the white polygon represents the study area.

The mechanism by which eddies change pCO_2 is similar to that explained for the STF movement, and eddies are also closely related to the frontal process. Eddies can transport water masses across fronts (Moreau et al., 2017; Patel et al., 2019, 2020). During the heterotrophic season of 2019, several cyclonic eddies with a warm core (identified by negative SLA) moved into our study region from the north (Figure 7c and f). Positive SST and SSS anomalies and negative MLD and pCO_2-NT anomalies mostly coincided with the cyclones (Figure 6). A combination effect of STF movement and anticyclones influenced the SOTS area in 2015. From March to May, in 2015, the STF moved north, resulting in a similar phenomenon to 2009 described above (Figure 6). An anticyclone (positive SSH anomaly) was observed in July 2015, likely a result of the retreat of the STF in June and it moved to the northeast corner of our study region (Figure 7a and d). It briefly reversed the anomalies caused by SAZ water, drove a MLD deepening, reduced SST cooling and reduced pCO_2-NT (Figure 6 and 7).

Several eddies contributed to very dynamic conditions in 2016. Negative SST and positive pCO_2-NT anomalies occurred with a deeper MLD in May. The situation was reversed the next month. Two cyclones (one from the SAZ with a cold core, and one from STZ with a warm core) and one anticyclone lingered around the polygon during this period (Figure 7b, 7e and .mp4 movies in Supplementary Information for 2016). The cyclone-anticyclone interaction, and the potential vertical movement between them (Guidi et al., 2012) likely resulted in the time series variability in the heterotrophic season (Figure 6).

4. Discussion

4.1 Model validation

The pCO_2 computed by the MLR model (eq.1) correlates very well with the independent observations (refer to section 2.5). The seasonal cycle and the long-term trend were well captured ($p < 0.05$; Figure 3). The largest data-model discrepancy was between pCO_2-SOCCOM and pCO_2-MLR, especially in the winter of 2015 and 2016 (Figure 3). The estimated surface pCO_2 from profiling floats is over 400 μatm, about 30 μatm higher than pCO_2-MLR. In summer, pCO_2-MLR and pCO_2-SOCCOM coincide well. The SOCCOM observations could over-estimate pCO_2 by about 10 μatm (Gray et al., 2018; Williams et al., 2017), which might give the appearance of stronger outgassing in winter, but this is still not enough to explain the gap we observed in 2015. Other potential drivers of differences between observations and the model include spatial and temporal differences in sampling. Ships and floats only cover short periods during a month, and they are likely to be strongly influenced by local uptake or outgassing driven by small scale physical and biological perturbations. For the floats, the profiling interval of 10 days may miss or capture some important signals, resulting in biases (Bushinsky et al., 2019; Monteiro et al., 2015). The computed MLR is smoother at all points in the time series, compared to observations, which is a result of the monthly and regionally averaged predictor variables used as input. Our model may lose some sub-seasonal signals, but it simulates well the decadal trend and the seasonal cycle.

4.2 Seasonal variability and long-term increasing pCO_2

The seasonality of pCO_2-MLR is clear. It begins to decline before the autotrophic season and reaches its lowest value at the end of summer. The earlier decrease is probably the result of the early onset of phytoplankton growth, or MLD shoaling, or both before October (Figure S3). However, the negative correlation with chlorophyll concentration indicates that the pCO_2 decrease is mainly driven by primary productivity, especially in autotrophic seasons (Figure 3, 5 & S3; Rangama et al., 2005; Shadwick et al., 2015). Warming promotes the increase of pCO_2-T during the spring and summer, but this is masked by the biologically-driven decrease, which is much larger than the temperature effect (Figure 3 and S4; refer to section 3.2). The seasonal cycle of pCO_2-MLR is shaped like pCO_2-NT but with reduced amplitude. Earlier work at SOTS indicated a respiration signal of 40 µatm in the upper ocean after the autotrophic season, but the particulate organic carbon (POC) inventory at the end of summer was not enough to fuel it (Shadwick et al., 2015). This suggests that, besides remineralization, DIC-rich water mass input by upwelling or horizontal advection is also a major component of the rising of pCO_2-NT in the heterotrophic season (Figure 3; Pardo et al., 2019; Shadwick et al., 2015; Wang et al., 2001). Mesoscale structures were found to play an important role, and we will discuss these further in section 4.5.

The magnitude of the seasonal cycle in the pCO_2-MLR is broadly consistent with but slightly smaller than previous observations and gridded products in the SAZ (Borges et al., 2008; Shadwick et al., 2015; Takahashi et al., 2002). This is especially true for the high-precision observations from 2012 (Shadwick et al., 2015), and probably the result of the monthly averaging of our product. The seasonal magnitude changed little from 2004 to 2021, without a clear trend. The pCO_2 growth rate from 2004 to 2021 is about 2.8 µatm yr^{-1}, which is generally similar to previous research which documented increases of about 40 µatm from the late 1990s to 2012 (Metzl et al., 1999; Takahashi et al., 2002). The magnitude is also similar to the growth rate at the Hawaii Ocean Timeseries station in the North Pacific gyre (HOT; 2.4 µatm yr^{-1} from 2004 to 2013) but larger than recorded at Ocean Station Papa in the sub-Arctic Pacific (1.6 µatm yr^{-1} from 2007 to 2014), Stratus in the eastern tropical Pacific (2.0 µatm yr^{-1} from 2006 to 2015; Sutton et al., 2017) and the Bermuda Atlantic Time-series in the North Atlantic gyre (BATS; 1.8 µatm yr^{-1} from 1983 to 2011; Bates et al., 2014). In contrast, the atmospheric pCO_2 increased by 2.2 µatm yr^{-1}. From 2004 to 2021, the surface SST increased by 0.02 °C yr^{-1} (not shown), which would contribute about 0.28 µatm yr^{-1} to the growth of surface pCO_2 per year (Takahashi et al., 2002).

4.3 Air-sea CO_2 flux at SOTS

The magnitude of our MLR-based FCO_2 is broadly consistent with the observations at SOTS in 2012 (Figure 4; 1 to 20 mmol C m^{-2} d^{-1} reported in Shadwick et al. 2015), with the above-mentioned caveat around short-term variability. The magnitude of the SOTS region carbon sink is larger than the earlier observations and models that covered the more southern regions of the Indian Ocean sector of the Southern Ocean from ~60 °S to the seasonal sea ice zone (Borges et al., 2008; Gray et al., 2018; Lenton et al., 2013). The short outgassing period in August and September seems to be neglected in our MLR, which may suggest that SOTS, located in the northern SAZ, experiences weak outgassing that might be minimised in the monthly averages (Lenton et al., 2013; Shadwick et al., 2015). Between 2004 and 2011, FCO_2 increased, then gradually declined after 2011, consistent with the trend of Keppler & Landschützer (2019).

The negative relationship between the SAM index and FCO_2 (Table 1) is likely explained by the co-occurring increasing wind speed, which will increase the gas transfer velocity k in eq. 2. The average annual FCO_2 (into the ocean; negative) at the SOTS site (-6.0 mmol m^{-2} d^{-1}) is larger than at Station Papa (~ -2.7 mmol m^{-2} d^{-1}), at a similar latitude in the sub-Arctic North Pacific, and slightly smaller than that in the Kuroshio Extension Observatory (KEO) station (~ -6.5 mmol m^{-2} d^{-1}; Sutton et al., 2017). Outside the summer in the northern hemisphere, the KEO region is a strong carbon sink with a magnitude larger than about 20~30 mmol m^{-2} d^{-1} (Sutton et al., 2017), which is several times stronger than the SOTS region. But its annual carbon sink magnitude is only slightly larger than the SOTS region because of the strong seasonal outgassing (over 10 mmol m^{-2} d^{-1}) which is not observed at the SOTS site.

4.4 pCO_2 variability induced by SAM

The SOTS region has a weak response in general to the SAM. Different from previous global scale studies for the SAZ, our analysis indicates that the wind speed in the SOTS region strengthens with positive SAM with no time lag, rather than weakening with the poleward shift of the westerly winds (Table 1; Lenton & Matear, 2007; Lovenduski & Gruber, 2005). Stronger wind-driven mixing promotes mixed layer deepening with one month delay (Table 1). We have not detected any co-occurring SST or SSS anomalies, which lead us to rule out Ekman transport of southern water masses towards the north of the SAZ, to converge, sink and drive the MLD deepening (Lenton & Matear, 2007; Lovenduski & Gruber, 2005; Sallée et al., 2010). To some extent, this is in line with the pattern proposed by previous studies. That is, the SOTS site is located at the junction of areas where there will be significant positive and negative anomalies in response to the SAM, especially for SST and MLD (Lovenduski & Gruber, 2005; Sallée et al., 2010).

The biological component of the pCO_2 variability (pCO_2-NT) was positively correlated with the SAM with 4 months delay (Table 1). MLD or Chl did not respond similarly to SAM at the same time lag to explain the change in pCO_2-NT. This may be because Chl is not a good proxy for productivity outside the autotrophic season, because it is low and does not vary much. Chl is also always a positive number, so it is unable to reflect respiration, which is a major driver of increasing pCO_2. The change of pCO_2-NT represents the combination of biological processes (photosynthesis and respiration) and physical processes (advection, entrainment and mixing of seawater; Shadwick et al., 2015). The deep mixing, indicated by the positive MLD and negative SST anomalies, primarily increased pCO_2-NT during the heterotrophic season, while it was mainly reduced by phytoplankton in the autotrophic season (Figure 5; section 3.5). Recent research shows that the surface chlorophyll concentration in the Southern Ocean is difficult to correlate with low-frequency climate modes such as SAM (Prend et al., 2022). The slight positive correlation between the SAM and pCO_2 ($r = 0.15$) might be the combined result of variability of primary productivity and water mass movement, driven by the SAM, but not reflected by the correlation test with a single variable.

4.5 pCO_2 variability induced by mesoscale process

Through the case studies, we infer that ocean physics and biogeochemistry in the SOTS region were strongly affected by mesoscale activities. This region is located at the edge of the STF, which frequently meanders southward, and it is easily affected by the seasonal or interannual movement of the STF. Strong south-north gradients exist in the climatology of SST, SSS, MLD, Chl and pCO_2 (Figure 1; Borges et al., 2008; Bowie et al., 2009; Rangama et al., 2005). Therefore, when more saline and warmer water intrusions occur simultaneously with the southward movement of the STF, it is likely reflected at the SOTS site as the influence of subtropical water (Figure 6). The case study of 2009-2010 clearly demonstrated the influence of STF movement at the SOTS site (refer to section 3.6). In 2010, the northern water input (lower pCO_2, higher Chl; Borges et al., 2008) drove a sustained negative pCO_2 anomaly in the heterotrophic season (Figure 6). However, our analysis did not reveal enhanced heterotrophy outside the productive season acting to increase pCO_2-NT, unlike Shadwick et al. (2015). The STF movement dominated the local environment in this period, but other factors, like primary production (inferred via Chl) also influenced pCO_2. There was a positive Chl anomaly from February 2009 to June 2009, and this was likely the reason for the neutral pCO_2-NT, despite the input of DIC-rich subantarctic water (Figure 6). After the Chl anomaly returned to zero, pCO_2-NT increased.

This region is a generation site of long-lived eddies, and they play a vital role in transporting heat, salinity and nutrients (Dufour et al., 2015; Frenger et al., 2015; Patel et al., 2019, 2020; Sun et al., 2019). Eddy trapping (Frenger et al., 2015; McGillicuddy, 2016) will generally bring warmer and saltier water from the north or cooler and fresher water from the south. During the 6-year period of our 3 case studies, all the eddies formed in the STZ retained the warm core that they captured in the north, no matter if they were cyclones or anticyclones (.mp4 movies in Supplementary Information). Eddy pumping did not obviously change the cyclonic eddy SST anomaly to cool, despite it likely promoting upwelling to shoal the MLD, such as in June 2019 (Figure 6e, 7c, 7f and S5). Therefore, we relied on SLA (positive in anticyclones, negative in cyclones) to distinguish eddy type.

Eddy trapping contributes to transporting biogeochemical material, like biomass or carbon (Amos et al., 2019; Ito et al., 2010; Moreau et al., 2017). Eddies are also closely related to frontal movement, making this region very dynamic and unpredictable. Eddies can minimise the influence of STF movement, like during the heterotrophic season in 2015; or enhance the effect of STF movement, like in 2019. When there are multiple eddies involved, the physical and biogeochemical features are impacted by eddy interactions and could change very quickly, like in 2016. In our case, cyclones and anticyclones generated in the STZ all transported the trapped low DIC subtropical water from the north to the south, resulting in a pCO_2-NT decrease. This impact is opposite to the equatorward migration of a low productivity cyclone described in Moreau et al. (2017), which led local pCO_2 to increase and drove outgassing. But the underlying mechanism of eddy trapping is very similar. Eddy trapping is often the dominant mechanism in terms of driving physical and biogeochemical anomalies (Dufour et al., 2015; Gaube et al., 2013; Moreau et al., 2017). Here it has played a similar role to the STF movement, bringing northern waters into the SOTS region. Because eddy impacts occurred frequently with STF variability, it was often difficult to distinguish and attribute the contribution of each of them without detailed subsurface observations.

The variability of pCO_2 was also influenced by the deep mixing and primary productivity enhancement with short duration but high intensity (refer to section 3.6). The overlap of increasing pCO_2-NT and MLD deepening in November 2019 implied DIC-rich water being mixed to the surface. Then, it was rapidly consumed by the phytoplankton growth, and quickly drawn down by about 30 μatm in the next three months. The expected mesoscale eddy MLD anomalies did not correspond to Argo-based observations in all cases. Because the spatial scales of submesoscale eddy features (<10 km) are smaller than the resolution of satellite and Argo products (Calil et al., 2011; Guidi et al., 2012). We also postulate that the Argo float positions can induce error in the MLD gridded product. We observed several floats in anticyclones near SOTS, which might lead to deeper MLD estimations (Figure 6; .mp4 movies in Supplementary Information for 2019). Similarly, there were very few floats near the SOTS region in July 2009, and they all fell into cyclones (.mp4 movies in Supplementary Information for 2009). These MLD uncertainties will induce uncertainty in the pCO_2-MLR. Furthermore, as a strong driver of surface pCO_2 variability, Chl during the autotrophic season can be changed by mesoscale or submesoscale physics (Gaube et al., 2013; Guidi et al., 2012; Lévy et al., 2001), grazing pressure (Behrenfeld, 2010; Evans & Parslow, 1985), light and nutrient availability (Behrenfeld, 2010; Eveleth et al., 2017; Lannuzel et al., 2011) or interaction between these (Prend et al., 2022). Increasing evidence suggests that interseasonal activities like storms are also likely to induce short but intense air-sea flux anomalies (Monteiro et al., 2015; Nicholson et al., 2022). These variabilities have impacts on surface pCO_2, which can explain its weak connection with the low-frequency SAM. For the SOTS region, understanding small-scale and sub-seasonal processes is likely needed to capture the regional carbon variability more accurately.

Conclusions

By constructing and evaluating a time series of pCO_2 over the past two decades, we improve the understanding of the seasonal cycle and the contributions of physical and biological processes in the Subantarctic region of the Southern Ocean. The magnitude of the pCO_2 seasonal cycle is about 44 µatm. It varied from 30 to 54 µatm from 2004 to 2021, and the contribution of biological processes to seasonal variability was several times larger than thermal processes. From 2004 to 2021, this region acted as a net atmospheric CO_2 sink with an average magnitude of 6.0 mmol m^{-2} d^{-1}. Correlation tests suggested that the ocean uptake of CO_2 is slightly increased by stronger winds, which are enhanced by a positive SAM index. Except for the weak impact of the climate mode, pCO_2 is predominantly changed by primary productivity during the autotrophic seasons. A group of case studies shows that water mass movement by mesoscale activities and associated with frontal migration is mainly responsible for the pCO_2 variability in the heterotrophic seasons. This study contributes to understanding the variability and trends of pCO_2 and helps to refine estimates of the magnitude of the oceanic sink for atmospheric CO_2 in the subantarctic zone. Further progress is needed to address the relationship between the local pCO_2 variability and small-scale and sub-seasonal high-frequency processes in this region, to understand their contribution to the climate system.

Open research

The observations collected at the SOTS site can be obtained from the Australian Ocean Data Network (AODN) portal: https://portal.aodn.org.au/search?uuid=723a3e85-04ae-40e6-ac2a-237a93d84abe. The 8-day surface chlorophyll data are available at the Ocean-Colour Climate Change Initiative (OC-CCI) via doi: 10.5285/1dbe7a109c0244aaad713e078fd3059a. The 8-day SST data for the same period are provided by NASA Goddard Space Flight Center at MODIS Aqua mission via doi: https://doi.org/10.5067/MODSA-8D4D9 and https://doi.org/10.5067/MODSA-8D4N9. SSH and wind speed at 10m data are provided by European Centre for Medium-Range Weather Forecasts (ECMWF) and the Copernicus Climate Change Service (C3S) via doi: 10.24381/cds.adbb2d47. The full-depth temperature, salinity and location of Argo floats are available at the International Argo Program and the national programs that contribute to it (http://www.argo.ucsd.edu, http://argo.jcommops.org). The Argo Program is part of the Global Ocean Observing System. The SSS data from ECMWF are available at

Integrated Climate Data Center: https://www.ecmwf.int/en/forecasts/dataset/ocean-reanalysis-system-5. The SOCCOM pCO_2 data can be obtained via doi: https://doi.org/10.6075/J0MC905G; the GLODAP pCO_2 data can be obtained at: https://www.glodap.info/index.php/merged-and-adjusted-data-product-v2-2022/; the SOCAT pCO_2 data are available at: https://www.socat.info/index.php/data-access/. The HPLC data from SOTS voyages are available in SOTS annual sample reports: https://catalogue-imos.aodn.org.au/geonetwork/srv/eng/catalog.search#/metadata/afc166ce-6b34-44d9-b64c-8bb10fd43a07 and the AODN at IMOS Satellite Remote Sensing- Ocean Colour - Bio Optical Database of Australian Waters (SRS-OC-BODBAW). The voyage details are listed in Table S1 in the Supporting Information. Atmospheric mole fractions of CO_2 was measured at the Kennaook / Cape Grim Baseline Air Pollution Station (KCGBAPS), which is funded and managed by the Australian Bureau of Meteorology, and the scientific program is jointly supervised with CSIRO Oceans & Atmosphere. The data can be obtained from: http://www.csiro.au/greenhouse-gases/. The SAM index is available at: https://legacy.bas.ac.uk/met/gjma/sam.html. The 'Air-sea CO_2 flux' Matlab function provided by: Cecilia Chapa (2022). Air-sea CO2 flux (https://www.mathworks.com/matlabcentral/fileexchange/50190-air-sea-co2-flux), MATLAB Central File Exchange. Retrieved October 12, 2022. The CO2SYS program is available at: https://github.com/jamesorr/CO2SYS-MATLAB. The Gibbs-SeaWater (GSW) Oceanographic Toolbox can be obtained at: https://www.teos-10.org/software.htm.

Acknowledgements

The SOTS mooring data was sourced from Australia's Integrated Marine Observing System (IMOS) – IMOS is enabled by the National Collaborative Research Infrastructure Strategy (NCRIS). This research was also supported by the Australian Antarctic Program Partnership through the Australian Government's Antarctic Science Collaboration Initiative. Pete Strutton is supported by the Australian Research Council Special Research Initiative, Australian Centre for Excellence in Antarctic Science (Project Number SR200100008). Xiang Yang gratefully acknowledges a PhD scholarship provided by China Scholarship Council (CSC) Grant (202106330009) from the Ministry of Education of the People's Republic of China.

Reference list

Amos, C. M., Castelao, R. M., & Medeiros, P. M. (2019). Offshore transport of particulate organic carbon in the California Current System by mesoscale eddies. *Nature Communications*, *10*(1), 1–8. https://doi.org/10.1038/s41467-019-12783-5

Argo. (2022). Argo float data and metadata from Global Data Assembly Centre (Argo GDAC) [Dataset]. SEANOE. https://doi.org/10.17882/42182

Bakker, D. C. E., Pfeil, B., Landa, C. S., Metzl, N., O'Brien, K. M., Olsen, A., et al. (2016). A multi-decade record of high-quality fCO2 data in version 3 of the Surface Ocean CO2 Atlas (SOCAT). Earth System Science Data, 8(2), 383–413. https://doi.org/10.5194/essd-8-383-2016

Bakker, D. C. E., Alin, S. R., Bates, N., Becker, M., Feely, R. A., Gkritzalis, T., et al. (2023). Surface Ocean CO2 Atlas Database Version 2023 (SOCATv2023) (NCEI Accession 0278913) [Data set]. NOAA National Centers for Environmental Information. https://doi.org/10.25921/R7XA-BT92

Bates, N. R., Astor, Y. M., Church, M. J., Currie, K., Dore, J. E., González-Dávila, M., et al. (2014). A time-series view of changing surface ocean chemistry due to ocean uptake of anthropogenic CO2 and ocean acidification. *Oceanography*, *27*(1), 126–141. https://doi.org/10.5670/oceanog.2014.16

Behrenfeld, M. J. (2010). Abandoning sverdrup's critical depth hypothesis on phytoplankton blooms. *Ecology*, *91*(4), 977–989. https://doi.org/10.1890/09-1207.1

Borges, A. V., Tilbrook, B., Metzl, N., Lenton, A., & Delille, B. (2008). Inter-annual variability of the carbon dioxide oceanic sink south of Tasmania. *Biogeosciences*, *5*(1), 141–155. https://doi.org/10.5194/bg-5-141-2008

Bowie, A. R., Lannuzel, D., Remenyi, T. A., Wagener, T., Lam, P. J., Boyd, P. W., et al. (2009). Biogeochemical iron budgets of the Southern Ocean south of Australia: Decoupling of iron and nutrient cycles in the subantarctic zone by the summertime supply. *Global Biogeochemical Cycles*, *23*(4), 1–14. https://doi.org/10.1029/2009GB003500

Bushinsky, S. M., Landschützer, P., Rödenbeck, C., Gray, A. R., Baker, D., Mazloff, M. R., et al. (2019). Reassessing Southern Ocean Air-Sea CO2 Flux Estimates With the Addition of Biogeochemical Float Observations. *Global Biogeochemical Cycles*, *33*(11), 1370–1388. https://doi.org/10.1029/2019GB006176

Calil, P. H. R., Doney, S. C., Yumimoto, K., Eguchi, K., & Takemura, T. (2011). Episodic upwelling and dust deposition as bloom triggers in low-nutrient, low-chlorophyll regions. *Journal of Geophysical Research: Oceans*, *116*(6), 1–16. https://doi.org/10.1029/2010JC006704

Chapa, C. (2023). Air-sea CO2 flux. [Software]. MATLAB Central File Exchange. https://www.mathworks.com/matlabcentral/fileexchange/50190-air-sea-co2-flux. Retrieved 10/02/2022.

Devries, T. (2014). The oceanic anthropogenic CO2 sink: Storage, air-sea fluxes, and transports over the industrial era. *Global Biogeochemical Cycles*, *28*(7), 631–647. https://doi.org/10.1002/2013GB004739

Dufour, C. O., Griffies, S. M., de Souza, G. F., Frenger, I., Morrison, A. K., Palter, J. B., et al. (2015). Role of mesoscale eddies in cross-frontal transport of heat and biogeochemical tracers in the Southern Ocean. *Journal of Physical Oceanography*, *45*(12), 3057–3081. https://doi.org/10.1175/JPO-D-14-0240.1

Evans, G. T., & Parslow, J. S. (1985). A model of annual plankton cycles. *Deep Sea Research Part B. Oceanographic Literature Review*, *32*(9), 759. https://doi.org/10.1016/0198-0254(85)92902-4

Eveleth, R., Cassar, N., Sherrell, R. M., Ducklow, H., Meredith, M. P., Venables, H. J., et al. (2017). Ice melt influence on summertime net community production along the Western Antarctic Peninsula. *Deep-Sea Research Part II: Topical Studies in Oceanography*, *139*, 89–102. https://doi.org/10.1016/j.dsr2.2016.07.016

Fay, A.R., Gregor, L., Landschützer, P., McKinley, G.A., Gruber, N., Gehlen, M., Iida, Y., Laruelle, G.G., Rödenbeck, C., Roobaert, A., Zeng, J., 2021. SeaFlux: Harmonization of air-sea CO2 fluxes from surface pCO2 data products using a standardized approach. Earth Syst. Sci. Data 13, 4693–4710. https://doi.org/10.5194/essd-13-4693-2021

Frenger, I., Münnich, M., Gruber, N., & Knutti, R. (2015). Southern Ocean eddy phenomenology. *Journal of Geophysical Research: Oceans*, 2813–2825. https://doi.org/10.1002/2015JC011047.Received

Gaube, P., Chelton, D. B., Strutton, P. G., & Behrenfeld, M. J. (2013). Satellite observations of chlorophyll, phytoplankton biomass, and Ekman pumping in nonlinear mesoscale eddies. *Journal of Geophysical Research: Oceans*, *118*(12), 6349–6370. https://doi.org/10.1002/2013JC009027

Gray, A. R., Johnson, K. S., Bushinsky, S. M., Riser, S. C., Russell, J. L., Talley, L. D., et al. (2018). Autonomous Biogeochemical Floats Detect Significant Carbon Dioxide Outgassing in the High-Latitude Southern Ocean. *Geophysical Research Letters*, *45*(17), 9049–9057. https://doi.org/10.1029/2018GL078013

Gruber, N., Landschützer, P., & Lovenduski, N. S. (2019). The variable southern ocean carbon sink. *Science Advances*, *5*(4), 1–28. https://doi.org/10.1126/sciadv.aav6471

Guidi, L., Calil, P. H. R., Duhamel, S., Björkman, K. M., Doney, S. C., Jackson, G. A., et al. (2012). Does eddy-eddy interaction control surface phytoplankton distribution and carbon export in the North Pacific Subtropical Gyre? *Journal of Geophysical Research: Biogeosciences*, *117*(2), 1–12. https://doi.org/10.1029/2012JG001984

Hersbach, H., Bell, B., Berrisford, P., Biavati, G., Horányi, A., Muñoz Sabater, J., et al. (2018). ERA5 hourly data on single levels from 1959 to present. [Dataset] Copernicus Climate Change Service (C3S) Climate Data Store (CDS). https://doi.org/10.24381/cds.adbb2d47. Retrieved 02/05/2022.

IMOS (2022). IMOS - Deep Water Moorings - Southern Ocean Time Series (SOTS) - all delayed-mode data [Dataset]. Australian Ocean Data Network. https://portal.aodn.org.au/search?uuid=723a3e85-04ae-40e6-ac2a-237a93d84abe. Retrieved 01/04/2022.

Ito, T., Woloszyn, M., & Mazloff, M. (2010). Anthropogenic carbon dioxide transport in the Southern Ocean driven by Ekman flow. *Nature*, *463*(7277), 80–83. https://doi.org/10.1038/nature08687

Johnson, K. S., Riser, S. C., Talley, L. D., Sarmiento, J. L., Swift, D. D., Plant, J. N., et al. (2022). SOCCOM float data - Snapshot 2022-05-19. [Dataset] In Southern Ocean Carbon and Climate Observations and Modeling (SOCCOM) Float Data Archive. UC Retrieved 19/09/2022.San Diego Library Digital Collections. https://doi.org/10.6075/J0MC905G. Retrieved 30/06/2022.

Johnson, R., Strutton, P. G., Wright, S. W., McMinn, A., & Meiners, K. M. (2013). Three improved satellite chlorophyll algorithms for the Southern Ocean. *Journal of Geophysical Research: Oceans*, *118*(7), 3694–3703. https://doi.org/10.1002/jgrc.20270

Keppler, L., & Landschützer, P. (2019). Regional Wind Variability Modulates the Southern Ocean Carbon Sink. *Scientific Reports*, *9*(1), 1–10. https://doi.org/10.1038/s41598-019-43826-y

Key, R. M., Olsen, A., Van Heuven, S., Lauvset, S. K., Velo, A., Lin, X., et al. (2015). Global Ocean Data Analysis Project, Version 2 (GLODAPv2), ORNL/CDIAC-162, ND-P093 [Dataset]. Carbon Dioxide Information Analysis Center (CDIAC). https://doi.org/10.3334/CDIAC/OTG.NDP093_GLODAPV2

Landschützer, P., Gruber, N., Haumann, A., Rödenbeck, C., Bakker, D. C. E., Heuven, S. van, et al. (2015). The reinvigoration of the Southern Ocean carbon sink. *Science*, *349*, 1221–1224. https://doi.org/10.1126/science.aab2620

Landschützer, P., Gruber, N., Bakker, D.C.E., Stemmler, I., Six, K.D., 2018. Strengthening seasonal marine CO2 variations due to increasing atmospheric CO2. Nat. Clim. Chang. 8, 146–150. https://doi.org/10.1038/s41558-017-0057-x

Lannuzel, D., Bowie, A. R., Remenyi, T., Lam, P., Townsend, A., Ibisanmi, E., et al. (2011). Distributions of dissolved and particulate iron in the sub-Antarctic and Polar Frontal Southern Ocean (Australian sector). *Deep-Sea Research Part II: Topical Studies in Oceanography*, *58*(21–22), 2094–2112. https://doi.org/10.1016/j.dsr2.2011.05.027

Le Quéré, C., Rödenbeck, C., Buitenhuis, E. T., Conway, T. J., Langenfelds, R., Gomez, A., et al. (2007). Saturation of the southern ocean CO2 sink due to recent climate change. Science, 316(5832), 1735–1738. https://doi.org/10.1126/science.1136188

Lenton, A., & Matear, R. J. (2007). Role of the Southern Annular Mode (SAM) in Southern Ocean CO2 uptake. *Global Biogeochemical Cycles*, *21*(2), 1–17. https://doi.org/10.1029/2006GB002714

Lenton, A., Tilbrook, B., Law, R. M., Bakker, D., Doney, S. C., Gruber, N., et al. (2013). Sea-air CO2 fluxes in the Southern Ocean for the period 1990-2009. *Biogeosciences*, *10*(6), 4037–4054. https://doi.org/10.5194/bg-10-4037-2013

Lévy, M., Klein, P., & Treguier, A. M. (2001). Impact of sub-mesoscale physics on production and subduction of phytoplankton in an oligotrophic regime. *Journal of Marine Research*, *59*(4), 535–565. https://doi.org/10.1357/002224001762842181

Lewis, E. R., & Wallace, D. W. R. (1998). Program Developed for CO2 System Calculations [Dataset]. Environmental System Science Data Infrastructure for a Virtual Ecosystem. https://doi.org/10.15485/1464255

Lovenduski, N. S., & Gruber, N. (2005). Impact of the Southern Annular Mode on Southern Ocean circulation and biology. *Geophysical Research Letters*, *32*(11), 1–4. https://doi.org/10.1029/2005GL022727

Lovenduski, N. S., Gruber, N., Doney, S. C., & Lima, I. D. (2007). Enhanced CO2 outgassing in the Southern Ocean from a positive phase of the Southern Annular Mode. *Global Biogeochemical Cycles*, *21*(2), 1–14. https://doi.org/10.1029/2006GB002900

Marshall, G. J. (2003). Trends in the Southern Annular Mode from observations and reanalyses. *Journal of Climate*, *16*(24), 4134–4143. https://doi.org/10.1175/1520-0442(2003)016<4134:TITSAM>2.0.CO;2

Marshall, G. J. (2022). An observation-based Southern Hemisphere Annular Mode Index

[Dataset]. https://legacy.bas.ac.uk/met/gjma/sam.html

McDougall, T.J. & Barker, P. M. (2011). *Getting started with TEOS-10 and the Gibbs Seawater (GSW) Oceanographic Toolbox*. [Toolbox]. SCOR/IAPSO WG127, ISBN 978-0-646-55621-5. Retrieved 12/01/2022.

McGillicuddy, D. J. (2016). *Mechanisms of Physical-Biological-Biogeochemical Interaction at the Oceanic Mesoscale*. *Annual Review of Marine Science* (Vol. 8). https://doi.org/10.1146/annurev-marine-010814-015606

McKinley, G. A., Takahashi, T., Buitenhuis, E., Chai, F., Christian, J. R., Doney, S. C., et al. (2006). North Pacific carbon cycle response to climate variability on seasonal to decadal timescales. *Journal of Geophysical Research: Oceans*, *111*(7), 1–22. https://doi.org/10.1029/2005JC003173

Metzl, N., Tilbrook, B., & Poisson, A. (1999). The annual f CO 2 cycle and the air’sea CO 2 flux in the sub-Antarctic Ocean . *Tellus B: Chemical and Physical Meteorology*, *51*(4), 849–861. https://doi.org/10.3402/tellusb.v51i4.16495

Monteiro, P. M. S., Gregor, L., Lévy, M., Maenner, S., Sabine, C. L., & Swart, S. (2015). Intraseasonal variability linked to sampling alias in air-sea CO2 fluxes in the Southern Ocean. *Geophysical Research Letters*, *42*(20), 8507–8514. https://doi.org/10.1002/2015GL066009

Moreau, S., Penna, A. Della, Llort, J., Patel, R., Langlais, C., Boyd, P. W., et al. (2017). Eddy-induced carbon transport across the Antarctic Circumpolar Current. *Global Biogeochemical Cycles*, *31*(9), 1368–1386. https://doi.org/10.1002/2017GB005669

NASA/JPL. (2020). MODIS Aqua Level 3 SST Thermal IR 8 Day 4km Daytime V2019.0 [Dataset]. NASA Physical Oceanography DAAC. https://doi.org/10.5067/MODSA-8D4D9. Retrieved 13/02/2022.

NASA/JPL. (2020). MODIS Aqua Level 3 SST Thermal IR 8 Day 4km Nighttime V2019.0 [Dataset]. NASA Physical Oceanography DAAC. https://doi.org/10.5067/MODSA-8D4N9. Retrieved 13/02/2022.

Nicholson, S. A., Whitt, D. B., Fer, I., du Plessis, M. D., Lebéhot, A. D., Swart, S., et al. (2022). Storms drive outgassing of CO2 in the subpolar Southern Ocean. *Nature Communications*, *13*(1), 1–12. https://doi.org/10.1038/s41467-021-27780-w

Orsi, A. H., Whitworth, T., & Nowlin, W. D. (1995). On the meridional extent and fronts of the Antarctic Circumpolar Current. *Deep-Sea Research Part I*, *42*(5), 641–673. https://doi.org/10.1016/0967-0637(95)00021-W

Pardo, P. C., Tilbrook, B., van Ooijen, E., Passmore, A., Neill, C., Jansen, P., et al. (2019).

Surface ocean carbon dioxide variability in South Pacific boundary currents and Subantarctic waters. *Scientific Reports*, *9*(1), 1–12. https://doi.org/10.1038/s41598-019-44109-2

Patel, R. S., Phillips, H. E., Strutton, P. G., Lenton, A., & Llort, J. (2019). Meridional Heat and Salt Transport Across the Subantarctic Front by Cold-Core Eddies. *Journal of Geophysical Research: Oceans*, *124*(2), 981–1004. https://doi.org/10.1029/2018JC014655

Patel, R. S., Llort, J., Strutton, P. G., Phillips, H. E., Moreau, S., Conde Pardo, P., & Lenton, A. (2020). The Biogeochemical Structure of Southern Ocean Mesoscale Eddies. *Journal of Geophysical Research: Oceans*, *125*(8), 1–24. https://doi.org/10.1029/2020JC016115

Prend, C. J., Keerthi, M. G., Lévy, M., Aumont, O., Gille, S. T., & Talley, L. D. (2022). Sub-Seasonal Forcing Drives Year-To-Year Variations of Southern Ocean Primary Productivity. *Global Biogeochemical Cycles*, *36*(7), 1–15. https://doi.org/10.1029/2022GB007329

Olsen, A., Key, R. M., van Heuven, S., Lauvset, S. K., Velo, A., Lin, X., et al. (2016). The Global Ocean Data Analysis Project version 2 (GLODAPv2) – an internally consistent data product for the world ocean. Earth System Science Data, 8(2), 297–323. https://doi.org/10.5194/essd-8-297-2016

Rangama, Y., Boutin, J., Etcheto, J., Merlivat, L., Takahashi, T., Delille, B., et al. (2005). Variability of the net air-sea CO2 flux inferred from shipboard and satellite measurements in the Southern Ocean south of Tasmania and New Zealand. *Journal of Geophysical Research: Oceans*, *110*(9), 1–17. https://doi.org/10.1029/2004JC002619

Roemmich, D., & Gilson, J. (2009). The 2004-2008 mean and annual cycle of temperature, salinity, and steric height in the global ocean from the Argo Program. *Progress in Oceanography*, *82*(2), 81–100. https://doi.org/10.1016/j.pocean.2009.03.004

Roesler, C., Uitz, J., Claustre, H., Boss, E., Xing, X., Organelli, E., et al. (2017). Recommendations for obtaining unbiased chlorophyll estimates from in situ chlorophyll fluorometers: A global analysis of WET Labs ECO sensors. *Limnology and Oceanography: Methods*, *15*(6), 572–585. https://doi.org/10.1002/lom3.10185

Sabine, C. L., Feely, R. A., Gruber, N., Key, R. M., Lee, K., Bullister, J. L., et al. (2004). The Oceanic Sink for Anthropogenic CO2, *305*(July), 5–12.

Sabine, C. L., Hankin, S., Koyuk, H., Bakker, D. C. E., Pfeil, B., Olsen, A., et al. (2013). Surface Ocean CO2 Atlas (SOCAT) gridded data products. Earth System Science Data, 5(1), 145–153. https://doi.org/10.5194/essd-5-145-2013

Sallée, J. B., Speer, K. G., & Rintoul, S. R. (2010). Zonally asymmetric response of the Southern Ocean mixed-layer depth to the Southern Annular Mode. *Nature Geoscience*, *3*(4), 273–279. https://doi.org/10.1038/ngeo812

Sarmiento, J. L., Gruber, N., Brzezinski, M. A., & Dunne, J. P. (2004). High-latitude controls of thermoclinenutrients and low latitudebiological productivity. *Nature*, *427*(6969), 56–60. https://doi.org/10.1038/nature02204.1.

Sathyendranath, S., Jackson, T., Brockmann, C., Brotas, V., Calton, B., Chuprin, A., et al. (2021). ESA Ocean Colour Climate Change Initiative (Ocean_Colour_cci): Version 5.0 Data [Dataset]. NERC EDS Centre for Environmental Data Analysis. https://doi.org/10.5285/1DBE7A109C0244AAAD713E078FD3059A. Retrieved 04/05/2022.

Schallenberg, C., Harley, J. W., Jansen, P., Davies, D. M., & Trull, T. W. (2019). Multi-year observations of fluorescence and backscatter at the southern ocean time series (SOTS) shed light on two distinct seasonal bio-optical regimes. *Frontiers in Marine Science*, *6*(SEP), 1–19. https://doi.org/10.3389/fmars.2019.00595

Shadwick, E. H., Trull, T. W., Tilbrook, B., Sutton, A. J., Schulz, E., & Sabine, C. L. (2015). Seasonality of biological and physical controls on surface ocean CO2 from hourly observations at the Southern Ocean Time Series site south of Australia. *Global Biogeochemical Cycles*, *29*(2), 223–238. https://doi.org/10.1002/2014GB004906

Shadwick, E. H., Rigual-Hernández, A. S., Eriksen, R. S., Jansen, P., Davies, D. M., Wynn-Edwards, C. A., et al. (2021). Changes in Southern Ocean Biogeochemistry and the Potential Impact on pH-Sensitive Planktonic Organisms. *Oceanography*, *34*(4), 14–15. https://doi.org/10.5670/oceanog.2021.supplement.02-06

Sokolov, S., & Rintoul, S. R. (2002). Structure of Southern Ocean fronts at 140°E. *Journal of Marine Systems*, *37*(1–3), 151–184. https://doi.org/10.1016/S0924-7963(02)00200-2

Steele, L. P., P. B. Krummel, M. V. van der Schoot, D. A. Spencer, Z. M. Loh, S. B. Baly et al. (2021). Baseline carbon dioxide monitoring, in Baseline Atmospheric Program (Australia) 2011-2013 [Dataset]. Australian Bureau of Meteorology and CSIRO Oceans and Atmosphere, Melbourne, Australia. https://doi.org/10.25919/mp7r-1v15

Sun, B., Liu, C., & Wang, F. (2019). Global meridional eddy heat transport inferred from Argo and altimetry observations. *Scientific Reports*, *9*(1), 1–10. https://doi.org/10.1038/s41598-018-38069-2

Sutton, A. J., Feely, R. A., Sabine, C. L., McPhaden, M. J., Takahashi, T., Chavez, F. P., et al. (2014). Natural variability and anthropogenic change in equatorial Pacific surface ocean pCO2 and pH. *Global Biogeochemical Cycles*, *28*(2), 131–145. https://doi.org/10.1002/2013GB004679

Sutton, A. J., Wanninkhof, R., Sabine, C. L., Feely, R. A., Cronin, M. F., & Weller, R. A. (2017). Variability and trends in surface seawater pCO2 and CO2 flux in the Pacific Ocean. *Geophysical Research Letters*, *44*(11), 5627–5636. https://doi.org/10.1002/2017GL073814

Sutton, A.J., Battisti, R., Carter, B., Evans, W., Newton, J., Alin, S., Bates, N.R., Cai, W.J., Currie, K., Feely, R.A., Sabine, C., Tanhua, T., Tilbrook, B., Wanninkhof, R., 2022. Advancing best practices for assessing trends of ocean acidification time series. Front. Mar. Sci. 9, 1–14. https://doi.org/10.3389/fmars.2022.1045667

Takahashi, T., Sutherland, S. C., Sweeney, C., Poisson, A., Metzl, N., Tilbrook, B., et al. (2002). Global sea-air CO2 flux based on climatological surface ocean pCO2, and seasonal biological and temperature effects. *Deep-Sea Research Part II: Topical Studies in Oceanography*, *49*(9–10), 1601–1622. https://doi.org/10.1016/S0967-0645(02)00003-6

Takahashi, T., Sutherland, S. C., Wanninkhof, R., Sweeney, C., Feely, R. A., Chipman, D. W., et al. (2009). Climatological mean and decadal change in surface ocean pCO2, and net sea-air CO2 flux over the global oceans. *Deep-Sea Research Part II: Topical Studies in Oceanography*, *56*(8–10), 554–577. https://doi.org/10.1016/j.dsr2.2008.12.009

Trull, T. W., Bray, S. G., Manganimi, S. J., Honjo, S., & François, R. (2001). Moored sediment trap measurements of carbon export in the Subantartic and Polar Frontal Zones of the Southern Ocean, south of Australia. *Journal of Geophysical Research*, *106*(2000), 31,489-31,509.

Van Heuven, S., Pierrot, D., Rae, J. W. B., Lewis, E., & Wallace, D. W. R. (2011). MATLAB Program Developed for CO2 System Calculations. ORNL/CDIAC-105b. [Software]. Carbon Dioxide Information Analysis Center (CDIAC). https://doi.org/10.3334/CDIAC/OTG.CO2SYS_MATLAB_V1.1. Retrieved 10/03/2022.

Vives, C. R., Schallenberg, C., Strutton, P. G., & Westwood, K. J. (2022). Iron and light limitation of phytoplankton growth off East Antarctica. *Journal of Marine Systems*, *234*(July 2021), 103774. https://doi.org/10.1016/j.jmarsys.2022.103774

Wang, X., Matear, R. J., & Trull, T. W. (2001). Modeling seasonal phosphate export and resupply in the Subantarctic and Polar Frontal Zones in the Australian sector of the Southern Ocean. *Journal of Geophysical Research C: Oceans*, *106*(2000), 525–541. https://doi.org/https://doi.org/10.1029/2000JC000645

Weiss, R. F. (1974). Carbon dioxide in water and seawater: the solubility of a non-ideal gas. *Marine Chemistry*, 203–215. https://doi.org/https://doi.org/10.1016/0304-4203(74)90015-2

Williams, N. L., Juranek, L. W., Feely, R. A., Johnson, K. S., Sarmiento, J. L., Talley, L. D., et al. (2017). Calculating surface ocean pCO2 from biogeochemical Argo floats equipped with pH: An uncertainty analysis. *Global Biogeochemical Cycles*, *31*(3), 591–604. https://doi.org/10.1002/2016GB005541

Wright, S. W., van den Enden, R. L., Pearce, I., Davidson, A. T., Scott, F. J., & Westwood, K. J. (2010). Phytoplankton community structure and stocks in the Southern Ocean (30-80°E) determined by CHEMTAX analysis of HPLC pigment signatures. *Deep-Sea Research Part II: Topical Studies in Oceanography*, *57*(9–10), 758–778. https://doi.org/10.1016/j.dsr2.2009.06.015

Wynn-Edwards, C. A., Davies, D. M., Eriksen, R. S., Jansen, P., Trull, T. W., & Shadwick, E. H. (2020a). Southern Ocean Time Series SOTS Annual Reports: 2016/2017 Report 2. Samples Version 1.0. https://doi.org/10.26198/mbf0-ry85

Wynn-Edwards, C. A., Davies, D. M., Jansen, P., Shadwick, E. H., & Trull, T. W. (2020b). Southern Ocean Time Series SOTS Annual Reports: 2018/2019 Report 2. Samples Version 1.0. https://doi.org/10.26198/r9ny-r549

Wynn-Edwards, C. A., Davies, D. M., Eriksen, R., Jansen, P., Bray, S. G., Shadwick, E. H., & Trull, T. W. (2021). Southern Ocean Time Series SOTS Annual Reports: 2013/2015 Report 2. Samples Version 1.0. https://doi.org/10.26198/6504-se58

Wynn-Edwards, C. A., Davies, D. M., Eriksen, R. S., Jansen, P., Trull, T. W., & Shadwick, E. H. (2022). Southern Ocean Time Series SOTS Annual Reports: 2020/2021 Report 2. Samples Version 1.0. https://doi.org/10.26198/wsf3-9r77

Wynn-Edwards, C. A., Shadwick, E. H., Davies, D. M., Bray, S. G., Jansen, P., Trinh, R., & Trull, T. W. (2020). Particle Fluxes at the Australian Southern Ocean Time Series (SOTS) Achieve Organic Carbon Sequestration at Rates Close to the Global Median, Are Dominated by Biogenic Carbonates, and Show No Temporal Trends Over 20-Years. *Frontiers in Earth Science*, *8*(August). https://doi.org/10.3389/feart.2020.00329

Yang, X., Strutton, P. G., Cyriac, A., Phillips, H. E., Pittman, N. A., & Vives, C. R. (2022). Physical Drivers of Biogeochemical Variability in the Polar Front Meander. *Journal of Geophysical Research: Oceans*, *127*(6), 1–19. https://doi.org/10.1029/2021JC017863

Zeebe, R. E., & Wolf-Gladrow, D. A. (2001). CO_2 in seawater: equilibrium, kinetics, isotopes. Amsterdam ; New York: Elsevier.

Zuo, H., Balmaseda, M. A., Tietsche, S., Mogensen, K., & Mayer, M. (2019). The ECMWF operational ensemble reanalysis–analysis system for ocean and sea ice: a description of the system and assessment. Ocean Science, 15(3), 779–808. https://doi.org/10.5194/os-15-779-2019